Helium ray-tracing

Simulating the neutral helium atom microscope NEMI using McStas

by Anders Komár Ravn *(sdz360)*

Submitted to the Faculty of Science at
the University of Copenhagen
in partial fulfillment of the degree of
Bachelor of Science in the subject of Physics.

June 10, 2015

Supervisors:

Kim Lefmann, Niels Bohr Institute, University of Copenhagen, Denmark

Bodil Holst, Department for Physics and Technology, University of Bergen, Norway

Erik B. Knudsen, DTU Physics, Technical University of Denmark, Denmark

Abstract

This thesis investigates the validity of making simulations of neutral matter-wave microscope instrumentation, by modifying the well established McStas neutron ray tracing software. Specifically this thesis models the neutral helium atom microscope, NEMI, located at the University of Bergen. Two new instrument components were written in order to simulate NEMI. The new components were a source with a Lorentzian wavelength distribution and Gaussian spatial distribution, and a Fresnel zone plate. The simulations comply with the physics intended to be simulated, and show a subtle, but important, dependency on wavelength that was not present in previous geometrical calculations done by the NEMI group in Bergen.

Dansk resumé

Dette bachelorprojekt undersøger gyldigheden af at lave simulationer af neutral stof-bølgemikroskopinstrumentering, ved at modificere det veletablerede McStas neutron ray-tracing software. Konkret handler denne afhandling om at modellere det neutrale helium atom mikroskop, NEMI, der står ved Universitetet i Bergen. To nye instrument komponenter blev skrevet for at simulere NEMI. De nye komponenter var en kilde med en Lorentz-fordeling i bølgelængder og en Gaussisk rumlig fordeling, og en Fresnel zone plade. Simuleringerne overholder den kendte fysik bag komponenterne, og viser en subtil, men dog vigtig, afhængighed af bølgelængde, der ikke var til stede i tidligere geometriske beregninger udført af NEMI-gruppen i Bergen.

ACKNOWLEDGEMENTS

Contents

1. Introduction

Microscopy has for long been a key method for scientists to study and observe features smaller than the naked eye can see. In the 16th century the first microscopes were constructed[17]. They were optical in design where light would be scattered by the object being studied and focused through an optical lens system to the eye of the observer. To this day microscopes have been a key tool in answering fundamental questions set by investigators of the physical world.

We have come a long way since the earliest microscopes, however, and there have been many landmark achievements in the field of microscopy in recent years. The prime objective of most modern research in microscopy techniques is to find ways to overcome or circumvent the Abbe resolution limit. Abbe discovered back in 1837 that light with wavelength λ travelling in a medium with refractive index n converging on a spot with the angle θ will make a spot with radius $d = \lambda/2n\sin\theta$ for optical microscopes[14]. In 2014 the Nobel prize in chemistry was given to William Moerner, Erik Betzig and Stefan Hell [15] for their work and contribution to the field of super resolution microscopy[1], especially the development of several kinds of stimulated emission depletion microscopy (STED) where, with a clever use of so-called excitation and depletion lasers, fluorophores in the sample of interest can be observed in high detail.

Examples of non-optical microscopes is scanning probe microscopes (SPM) such as the atomic force microscope (AFM) and the scanning tunnelling microscope (STM)[10]. These SPM microscopes works by recording the interaction between a sharp tip and a sample, either by measuring the change in current at a constant height or vice versa in the case of STM; or by measuring the inter-atomic forces between the tip and surface of the sample in the case of ATM. In either case only samples of a certain smoothness and stiffness are easy to image in a quickly and reliable manner. If the sample is too soft or rough, or has a high aspect ratio, then a slow scanning speed is required to get an image and not damage the sample or tip.

Another type of microscope is the matter-wave microscopes such as the scanning electron microscope (SEM/ESEM) and the transmission electron microscope (TEM)[6], and the very new helium-ion microscope (HIM)[11]. In TEM images are taken of electrons transmitted through very thin samples. In SEM and ESEM the image is recorded from the backscattered and secondary electrons exited from the sample. Normally samples used in these microscopes have to be conducting,

---

[1]A common denomination for all optical techniques that in some way or other bypasses the Abbe limit.

otherwise the sample may get charged and that distorts the image, and the sample may also get damaged by heating or ionization.

All in all these microscopes are very useful and powerful techniques to overcome the problem with the Abbe limit for optical microscopes, however, most of these require the samples in question to be either very smooth, sturdy, conducting or a combination of these requirements.

In the interest of coming up with a technique with the ability to fast and reliably image fragile, insulating samples with high aspect ratios, researchers came up with the idea of microscopes based on neutral atom or molecule beams scattering. Even though this notion is not new, the technical realization of such an instrument has proven to be a challenge. The very nature of neutral matter-waves dictate for them to be focused requires they are manipulated through their de Broglie wavelength. This has to be done analogous to classical optics since neutral atoms do not interact with the electro- and magneto-optical lenses used in electron and ion microscopes. Since low-energy molecules do not penetrate solid matter, lenses are out, and the only two focusing elements left are Fresnel zone plates and mirrors. The first images obtained using a neutral helium beam was in 2007 by Koch et al.[12]. The focusing element in their set-up was a Fresnel zone plate.

The Neutral Microscope, NEMI[2], is one of these neutral matter-wave microscopes. NEMI is located at the Department for Physics and Technology at the University of Bergen.

The aim of this work is to simulate the Neutral Microscope, using the neutron ray-tracing tool McStas by a modification of the program to simulate helium physics, and verify the simulation with experimental data taken with the NEMI instrument. The NEMI team is particularly interested in finding out what the smallest achievable focus is at a certain speed distribution when using a zone plate as the focusing element. Simple geometrical models are not accurate enough. It should be mentioned that this project is the first steps toward a planned expansion of McStas into McHe (working title), a ray-tracing software package to simulate helium beam experiments.

2. NEMI

The Neutral Microscope, NEMI for short, is a *reflecting neutral matter-wave scanning microscope* that uses neutral ground-state helium-4 as the probing beam.

---

[2]Although the acronym never was in question, what it's an acronym of is a matter of taste. Examples are: neutral helium atom microscope, neutral matter-wave microscope and neutral helium scattering microscope, and the list goes on.

It works in principle similarly to an SEM, creating an image by scanning the focused beam across a sample. In this case this is achieved by having movable sample stage which can rotate and translate for the beam to scan. The image is a record of the backscattered atoms by a detector placed at an angle from the optical axis. FIGURE 2.1 is a conceptual drawing of this.

Nozzle

Skimmer

Collimating Aperture

g=935 mm

He-Beam

Zone Plate

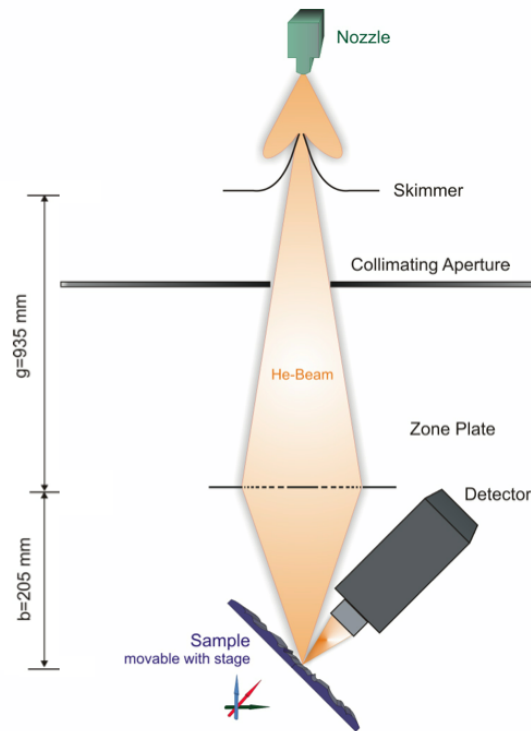Detector

b=205 mm

Sample
movable with stage

FIGURE 2.1: Schematic drawing of the working principle of NEMI. The source is on a typical *nozzle* mounted on a cooling block through which a high-pressure tube runs. A *skimmer* selects the central part of the beam to be imaged onto the *sample* by the *zone plate*. Between the nozzle and skimmer is low pressure, and beyond the skimmer everything is in vacuum. Image taken from [5] by Eder.

The main components on NEMI is the beam source, the skimmer, the optical element and the detection system.

The beam source is in principle no different from the sources found in other modern helium atom scattering devices. It produces a beam by expanding a high-pressure helium gas through a small nozzle aperture into a low-pressure ambient chamber[5]. By choosing the right nozzle diameter, gas pressure and temperature a so called free-jet expansion can be achieved, resulting in an almost monochromatic beam of neutral helium atoms[5, 16]. The distribution of wavelengths is Lorentzian,

and is characterized by the speed ratio[5]

$$S = 2\sqrt{\ln 2}\,\frac{\bar{v}}{\Delta v},$$

where $\bar{v}$ is the mean velocity of the atoms, and Δv is the FWHM of the speed distribution[4, 5, 12]. It is shown in [5] that the FWHM of the Lorentzian wavelength distribution can be expressed as

$$\Delta\lambda = 2\sqrt{\ln 2}\,\lambda_0 S^{-1}, \tag{1}$$

where λ_0 is the median and mode of the distribution.

The skimmer is the beam shaping element. It has a conical shape with a small orifice at the source-facing side. FIGURE 2.2 is a photograph of the skimmer used in NEMI. The skimmer has several functions in the microscope: (i) It separates the source chamber and the pumping stage vacuum chamber thereby working as a differential pumping stage. (ii) It confines the helium beam – it restricts the spatial intensity distribution of the free-jet expansion. And finally (iii) the skimmer diameter defines the object size which is being imaged by the zone plate[5].
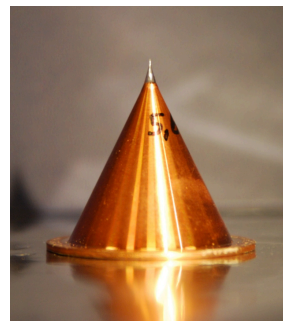
FIGURE 2.2: Photograph of the skimmer used in the NEMI instrument taken form [5]. The source-facing side (tip) has an opening with radius $5\,\mu m$.

The optical elements used to focus the beam is a Fresnel zone plate, as there is not a whole lot of alternatives as outlined in the introduction. The choice of zone plate instead of a mirror is simply because there are more technical limitations to using mirrors[3] and there have been several previous successful attempts at using a zone plate to focus a helium beam [3, 4, 12].

A Fresnel zone plate is a circular diffraction grating. FIGURE 2.3 is a sketch of a zone plate. The radius of the boundary between the n'th successive opaque and transparent rings on the zone plate is given by the formula

$$r_n^2 = n\lambda f + \frac{n\lambda}{4}, \tag{2}$$

---

[3]For a detailed technical description of this and more related to the construction of NEMI the author refers the reader to [5].
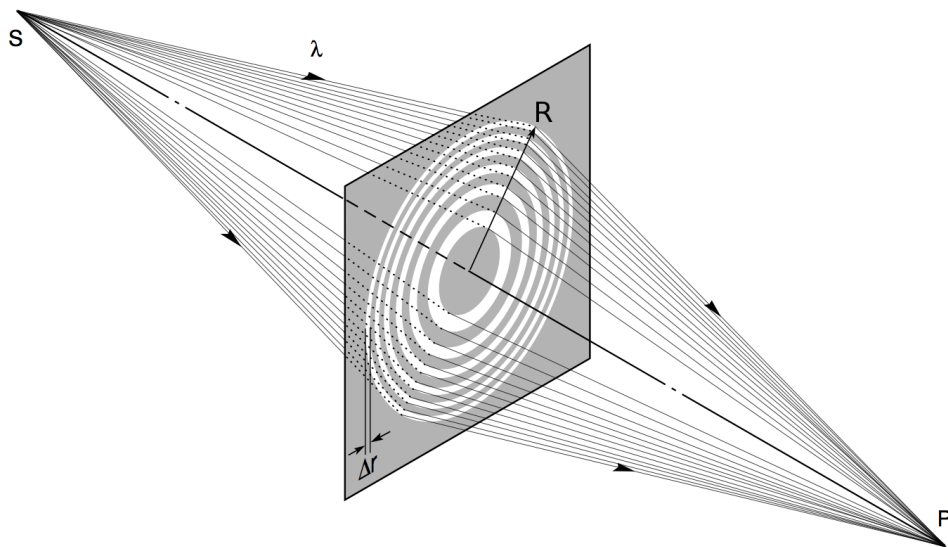
FIGURE 2.3: A sketch of the principle idea behind a Fresnel zone plate. Marked on the drawing is the radius R, the width of the outermost transmission zone Δr, the source at point S radiating waves of wavelength λ, which diffract on the grating to converge again in an image at point P. The distance to the image point is a function of all the marked parameters $P = P(S, R, \Delta r, \lambda)$. The image is taken from [1].

FIGURE 2.4: Sketch of the first three orders of focus in both convergent and divergent. Marked are the different focal and path lengths of the rays. Also drawn is a so-called order-sorting aperture (OSA), an aperture designed to sort out most rays of the other foci as to only let the first-order focused rays pass. Image taken from [1].

5

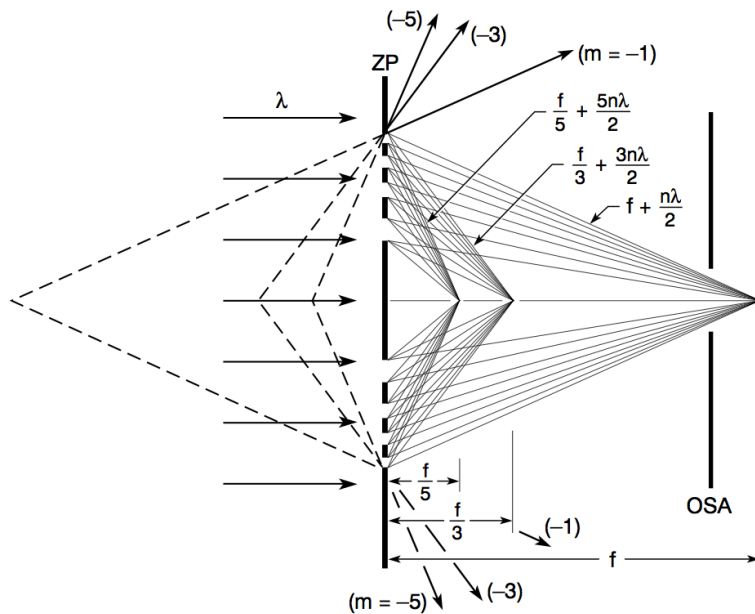where λ is the wavelength of the incoming wave and f is the focal length of the plate. The fractional term $n\lambda/4$ represents spherical aberration and is usually omitted since $f \gg n\lambda$ for most practical applications[1] including NEMI[5]. Equation (2) also imply that f is proportional to λ^{-1} i.e. a function of wavelength. Then, when the zone plate is exposed to waves with a distribution of wavelengths, chromatic aberration occurs, since each different wavelength will have a different focal length and therefore will be imaged at different positions[9]. As previously mentioned a Fresnel zone plate is a circular diffraction grating that can focus waves to a point. But unlike a lens, the transmission function allows for multiple foci. The transmission function can be expressed as a cosine series[1]

$$T(u) = \sum_{m=-\infty}^{\infty} c_m \cos mu,$$

where $u = \frac{\pi r^2}{f\lambda}$, m is the "order" and c_m is the Fourier component

$$c_m = \frac{1}{\pi} \int_0^{\frac{\pi}{2}} \cos mu \, \mathrm{d}u.$$

Now calculating the value of T for the different orders, m, shows that $50\,\%$ of the oncoming wave is reflected, $25\,\%$ pass through unchanged (the so-called 0-order beam), $10\,\%$ goes to the first-order focus, the same amount goes to the divergent first-order ($m = -1$) focus and $1\,\%$ to the third-order focus and so on[1]. FIGURE 2.4 is a drawing of the first orders of focus.
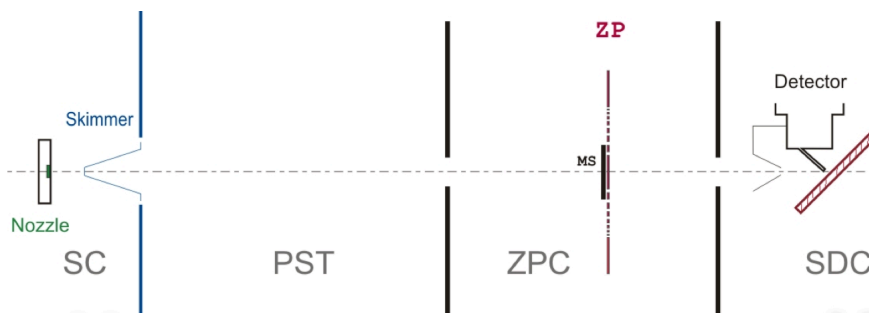
FIGURE 2.5: Sketch of the different pumping stages, from left to right: SC the source chamber, PST the pumping stage chamber, ZPC the zone plate chamber and SDC the sample and detector chamber. The black lines represent the dividing apertures. The image is taken from [5].

The detection system is a so called Pitot tube. The Pitot tube has a pinhole aperture. When the entering beam flow is equal to the effusive flow back out of the aperture, an equilibrium pressure can be measured. The change in pressure is

then taken as the measure of beam intensity[5].

In NEMI these are placed in different chambers separated by differential pumping stages. FIGURE 2.5 is an illustration of this. The first separation is, as previously mentioned, the skimmer between the source chamber and the pumping stage vacuum chamber. The zone plate chamber is isolated on either side by a 5 mm aperture separating it from the pumping stage vacuum chamber and the sample and the detector chamber.

3. MONTE CARLO SIMULATION USING MCSTAS

McStas is a software package developed specifically with the purpose of simulating neutron scattering experiments. Besides being a software package also a so called domain specific language (DLS) built on ANSI-C[19]. There are three levels of coding in McStas. The bottom level is the McStas kernel. This is where all low level particle transportation routines, geometry engines and such lay. It is written entirely in C, and also provides the basis for the MsStas DSL and compiler used on the other levels. The middle level is the component files. These files are the building blocks of the McSats simulated instruments. It is here on this level the Monte Carlo choices are taken. These files are for example beam sources, optical elements or detectors used in neutron scattering experiments. It is also on this level the samples are. The top level is the instrument files. The instrument files consist of a number of calls to different components, usually a source, then different optical components to manipulate the beam and finally a sample and detectors. This project works on the middle and top level.

3.1 RAY-TRACING, MCSTAS AND THE MONTE CARLO METHOD

Traditional ray-tracing methods, as the ones used to generate computer graphics, trace several rays from the eye through each pixel on the image frame to their sources and assign a value to the pixel based on sophisticated recursive algorithms taking into account material properties as well as reflections, refractions and shading[2, 7].

The McStas method is different. It utilises what is known as *backwards ray-tracing*[4] in the CG-business, tracing rays from the source to the image. The difference is that each ray's properties is determined by one or more Monte Carlo choices.

---

[4]According to [2]. [7] disagrees on the term for direction. The point is: McStas does it the opposite way of traditional ray-tracing for graphics rendering.

There is not just one Monte Carlo method. Looking up the encyclopedic definition[5] one finds that the Monte Carlo methods span a broad class of computer algorithms that rely on repeated random sampling to obtain numerical results. Monte Carlo methods typically follow a particular pattern:

1. Define a domain of possible inputs.

2. Generate inputs randomly from a probability distribution over the domain.

3. Perform a determistic computation on the input.

4. Aggregate the result.

At first glance this pattern is very clear in McStas: The end user defines the domain by setting the parameter values for the source. McStas then generates the actual simulation inputs with specific probability distribution in a number of parameters set in the source component and propagates the rays through the virtual instrument performing deterministic calculations at each component. Then finally it aggregates the result at a monitor which records either energies, wavelengths, position or some other parameter or parameters at the time the ray passed the monitor area. As an addendum to point number 3, it should be mentioned that McStas is also equipped to perform stochastic choices in a component or sample[13].

The Monte Carlo method used in McStas is a variation on the Monte Carlo integration method[19]. The Monte Carlo integration method[8] is a method to solve a multi-dimensional integral of the kind

$$I = \int_{\Omega} f(\underline{x}) \, \mathrm{d}\underline{x}$$

numerically using random numbers, where Ω is a subset of $\mathbb{R}^m$, $\int_{\Omega} \mathrm{d}\underline{x} = 1$ and f is square integrable on Ω. The Monte Carlo way to integrate such a function f is to generate N uniform samples $\underline{x}_1, \ldots, \underline{x}_N \in \Omega$ and approximate I by

$$E_N \equiv \frac{1}{N} \sum_{i=1}^{N} f(\underline{x}_i).$$

The law of large numbers is applicable, and shows

$$\lim_{N \to \infty} E_N = I.$$

---

[5]http://en.wikipedia.org/wiki/Monte_Carlo_method#Introduction

This, in turn, indicates that E_N is an unbiased estimator[8] of I, and the variance is

$$\sigma_{E_N}^2 = \frac{1}{N} \int_\Omega (f(\underline{x}) - I)^2 \, \mathrm{d}\underline{x} = \frac{\sigma_I^2}{N}.$$

In practice the true variance is rarely known and is therefore estimated by

$$s^2 = \frac{1}{N-1} \sum_{i=1}^{N} (f(\underline{x}_i) - E_N)^2 \tag{3}$$

3.2 THE McSTAS WEIGHT FACTOR

One of the fundamental concepts to understand when dealing with McStas is the so-called "weight factors". In the real world a neutron (or in this case a helium atom) is either present or lost, but, since only a fraction of the initial particles make it to the place where they are detected, McStas assigns each ray a weight factor. If for example the reflectivity of a certain component is $10\,\%$ and only the reflected rays are considered later in the simulation, the weight of every ray will be multiplied by 0.10 when passing the component and then reflected. This approach works around the problem of making a realistic simulation where only one in ten neutrons are reflected in the component.

Another way of expressing this, is by saying, if the real life probability of an outcome ϵ of an interaction between a ray and a component is P_ϵ, and this particular outcome is the only one of interest later in the simulation, the Monte Carlo probability of this outcome is set to one, $f_\epsilon = 1$, but the weight of the ray is multiplied by a weight multiplier π_ϵ, such that equation

$$\pi_\epsilon f_\epsilon = P_\epsilon \tag{4}$$

is always met, while keeping in mind

$$\sum_\epsilon P_\epsilon = \sum_\epsilon f_\epsilon = 1.$$

Equation (4) is called the fundamental multiplier law[13], and programmers should always bear this in mind when coding components for a McStas instrument.

The weight factor of a ray at any point is given by

$$w = w_0 \prod_{i=1}^{n} \pi_i,$$

where w_0 is the initial weight of the ray and this is multiplied by all weight multipliers of the previous components. McStas uses these weight factors to define the

intensity of rays at any given position (e.g. where the rays hits a detector) in the instrument like

$$I = \sum_j w_j, \tag{5}$$

where j is the ray index. Another way to write the intensity is $I = N\overline{w}$ where the bar denotes the arithmetic mean and N is the number of rays converging at that position.

When McStas records the intensity of a ray at a detector, it keeps track of three numbers N, I and σ_I^2. In order to calculate σ_I^2 it is easiest to look at (5) bearing in mind that there are deviations on both factors (and assuming they are statistically independent):

$$\sigma_I^2 = \sigma_N^2 \overline{w}^2 + N^2 \sigma_{\overline{w}}^2$$

Now harking the central limit theorem N is a counting number and therefore $\sigma_N^2 = N$, and all $w_j \approx \overline{w}$ which gives us

$$\sigma_I^2 = N(\overline{w}^2 + \sigma_{w_j}^2).$$

The true statistical variance of w_j is unknown but there exist an estimator $s_{w_j}^2 = s_{\overline{w}}^2 = \frac{1}{N-1}\left(\sum_j w_j^2 - N\overline{w}^2\right)$ akin to (3), which leads to

$$\sigma_I^2 \approx N(\overline{w}^2 + s_{\overline{w}}^2) = \frac{N}{N-1}\left(\sum_j w_j^2 - \overline{w}^2\right) \approx \sum_j w_j^2.$$

Now there is finally an expression for each of the numbers associated with a detection in McStas. These expressions are

$$N = \sum_j w_j^0 \qquad\qquad I = \sum_j w_j^1 \qquad\qquad \sigma_I^2 = \sum_j w_j^2. \tag{6}$$

4. Building NEMI in McStas

In order to simulate the NEMI instrument in McStas, the different components of NEMI have to exist. The components needed to investigate what happens at the focus of the beam in the instrument is a source, the optics (the apertures and zone plate) and detectors. I have chosen the four different types of components to be The current NEMI instrument file[6], and they are: A source[7], an aperture, a zone plate[8] and a detector. A schematic of the geometry of the simulated NEMI is presented in Figure 4.1.

---

[6]Source code in Appendix B.1
[7]Source code in Appendix B.2
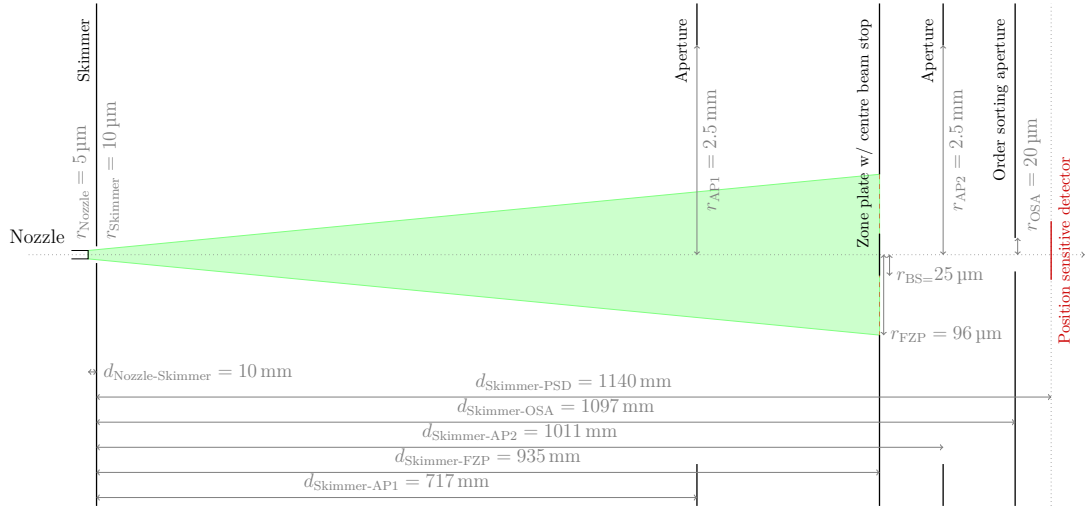[8]Source code in Appendix B.3

FIGURE 4.1: A visualisation of the simulated NEMI instrument, and the main distances and radii. The green cone represents the "focus" of most of the simulation runs. Only rays that fit within the cone are simulated. The two apertures functioning as differential pumping stages in the real instruments are implemented for completion but not needed to simulate the instrument. A position sensitive detector (PSD) is placed where the sample would sit in the real instrument.

4.1 THE SOURCE

The component first written was the source of the helium atoms. The first thing to consider is the fact that McStas is built to handle neutrons not helium atoms, so the assumption made through out the project code is that neutral helium atoms behave just like neutrons that are four times heavier than usual – at least semi-classically. The source component "Source_Lorentz_He" is modelled after the "Source_Maxwell_3" component from the McStas component library[18], however modified greatly. Instead of simulating Maxwellian distribution in energy the helium source has to have a Gaussian intensity distribution in space over the output and a Lorentzian distribution in wavelengths to simulate the effects of the free-jet expansion happening at the nozzle[5].

The source component[9] need 4 kinds of input: (i) the geometry of the source, (ii) the geometry of and distance to the focus[10], (iii) information about the wavelength distribution and (iv) the spatial distribution and intensity. The way the

---

[9]A more detailed description can be found in Appendix A.2

[10]The term "focus" used here is the McStas slang word for an area on the unit sphere toward

code works is by having a ray output/source that can either be square, rectangular or circular. The circular option was added since the nozzle on NEMI has a circular aperture. When a ray is generated it is assigned a uniformly distributed random starting position, ρ_j, on the chosen source geometry and then the weight factor w_j is multiplied by a weight multiplier generated from a normalised Gaussian distribution over the geometry to accommodate the spatial distribution of a free-jet expansion. That weight multiplier is

$$\pi_{\mathcal{G}} = \frac{1}{2\sigma^2} \exp\left(\frac{-\rho_j^2}{\sigma\sqrt{2\pi}}\right).$$
(7)

Then the rays target is chosen from a uniform distribution on the focus geometry. Then the wavelength of the ray, λ_j, is chosen form a uniform distribution on the interval set by the user, and the weight factor is multiplied by a factor based on a Lorentzian wavelength distribution defined by $\gamma = {\Delta\lambda}/{2}$,

$$\pi_{\mathcal{L}} = \frac{1}{\pi\gamma} \frac{\gamma^2}{(\lambda_j - \lambda_0)^2 + \gamma^2}.$$
(8)

Finally the weight factor is multiplied by the penalties for the choices of source and focus geometry (SG and FG), and the flux parameter (I) to make sure that the weight factor has units of $\sec^{-1}$. All in all that provides the rays with a weight factor of

$$w_j = I \cdot \pi_{\mathcal{G}} \cdot \pi_{\mathcal{L}} \cdot \pi_{\mathrm{SG}} \cdot \pi_{\mathrm{FG}}.$$
(9)

when leaving the source.

4.2 The aperture

The "Aperture" component is a simple rip-off of the "Slit" component from [18]. This is a component that absorbs every ray outside a given area (circular or rectangular), while the rest carry on unchanged.

4.3 The Fresnel zone plate

The zone plate component[11] is approximated to a thin lens, to get around the fact that McStas is optimized for ray optics while the effect of a Fresnel zone plate lies

which the simulated rays propagate. The focus in this context chooses which rays are the "focus" of the simulation.

[11]Detailed description in Appendix A.1

in the realm of wave optics. It works by solving the matrix equation for a ray of light interacting with a thin lens[9]

$$\begin{bmatrix} x_{\text{out}} \\ \theta_{\text{out}} \end{bmatrix} = \begin{bmatrix} 1 & 0 \\ -1/f & 1 \end{bmatrix} \begin{bmatrix} x_{\text{in}} \\ \theta_{\text{in}} \end{bmatrix}, \tag{10}$$

where x is the radial intercept of the ray and zone plate, and θ is the angle of incidence, and substituting the focal length f with the focal length of a zone plate[1]

$$f = \frac{2R\Delta r}{\lambda}, \tag{11}$$

where R is the radius of the zone plate, Δr is the width of the outermost transmission zone and λ is the wavelength of the ray. Since only the first-order focused beam is simulated, the ray transmitted from the zone plate's weight factor is multiplied by a weight multiplier $\pi_{\text{ZP}} = 0.10$ to comply with the fundamental multiplier law (4). This is because the transmission function of a Fresnel zone plate states that only $10\,\%$ of the incoming wave is defracted to the first-order focus[1].

4.4 The detectors

The detectors used are the "PSD_monitor" and the "L_monitor" from [18]. The PSD monitor detects the positions of the rays on an area normal to the beam line, and the L monitor (read: lambda monitor) detects the wavelengths of the rays on an area normal to the beam line. The L monitor have been adjusted for helium detection.

5. Results and discussion

When referring to different wavelength distributions, I will use the term speed ratio, S, as a measure of the FWHM of the distributions. The relationship between the two quantities is stated in equation (1).

5.1 Sanity check

To check whether or not the code for the source behaves as intended, a simple instrument consisting of only the source and two detectors was scripted. Figure 5.1 illustrates how output of the nozzle is in fact Lorentzian in wavelength and Gaussian in space, and consistent with different parameter settings.
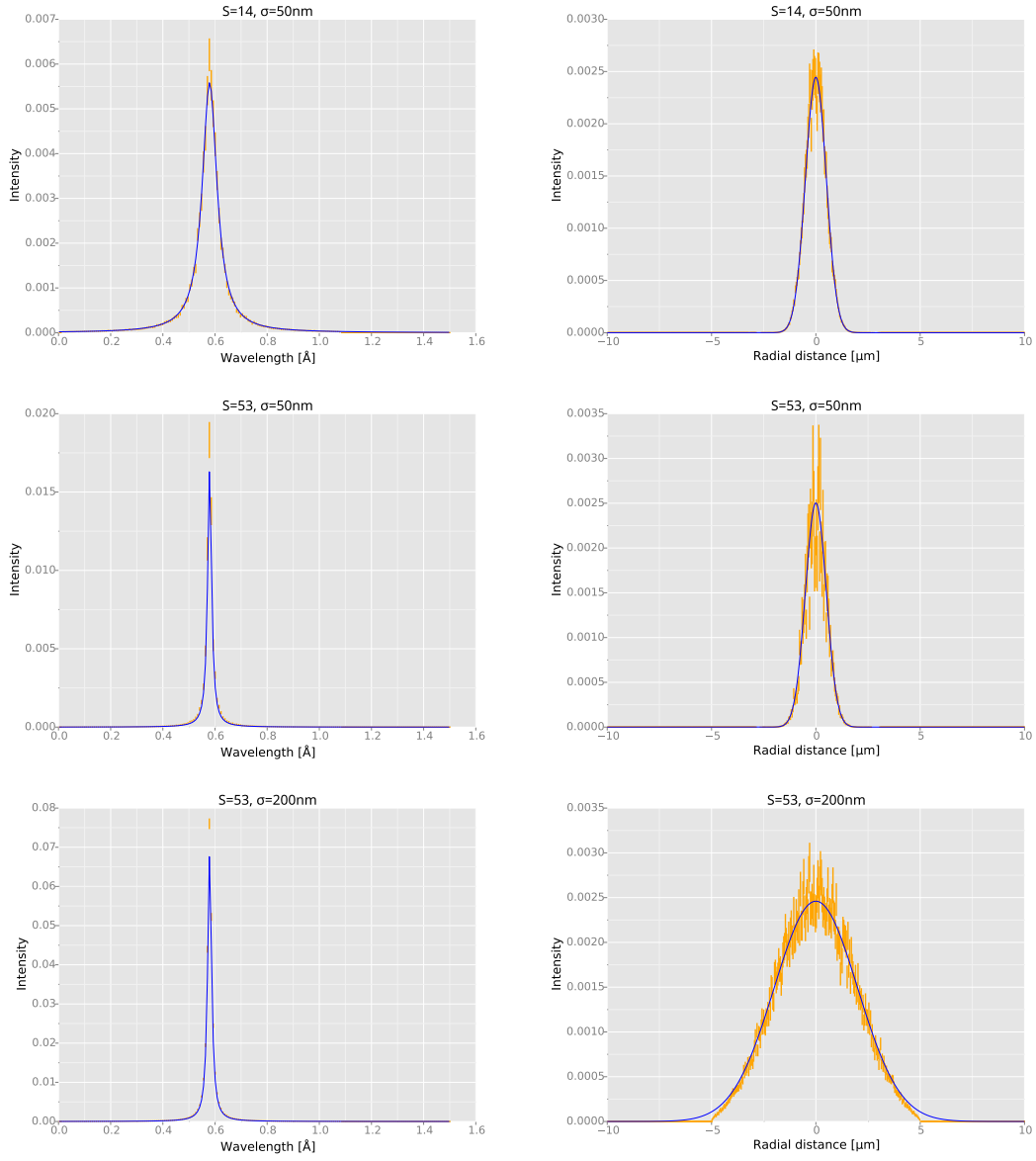
FIGURE 5.1: Characteristics of the beam from the source for three different nozzle settings, shown in the plot. Left column shows the wavelength distributions and right column shows the radial beam width. Simulated data with errors is shown in orange, while the blue lines are the expected distributions (Lorentzian and Gaussian, respectively). S is the speed ratio and σ is the width of the Gauss curve. The constant parameters are: $r_{\text{Nozzle}} = 5\,\mu\text{m}$ and $\lambda_0 = 0.579\,\text{Å}$

In order for the beam to be focused at 205 mm from the zone plate the corresponding wavelength had to be calculated. To do this f has to be isolated in (10), which yields

$$f = \frac{x}{\Delta\theta},$$

where $\Delta\theta$ is the beam's total change in angle[12]. Isolating λ in (11) produces an expression for the wavelength

$$\lambda = \frac{2R\Delta r}{x}\Delta\theta. \tag{12}$$

Using the zone plate parameters from the NEMI group, $x = R = 96\,\mu m$ and $\Delta r = 51\,nm$ reveals that the wavelength should be $\lambda_0 = 0.579\,\text{Å}$. To check if the zone plate actually focuses the beam at the expected point the NEMI instrument was coded[13] with the parameters specified in FIGURE 4.1 and the calculated wavelength. A series of detectors was placed around 205 mm from the zone plate to measure the spot size. FIGURE 5.2 shows that the beam does in fact converge at 205 mm and also that the effects of chromatic aberration is greater for a broader wavelength distribution, as expected.
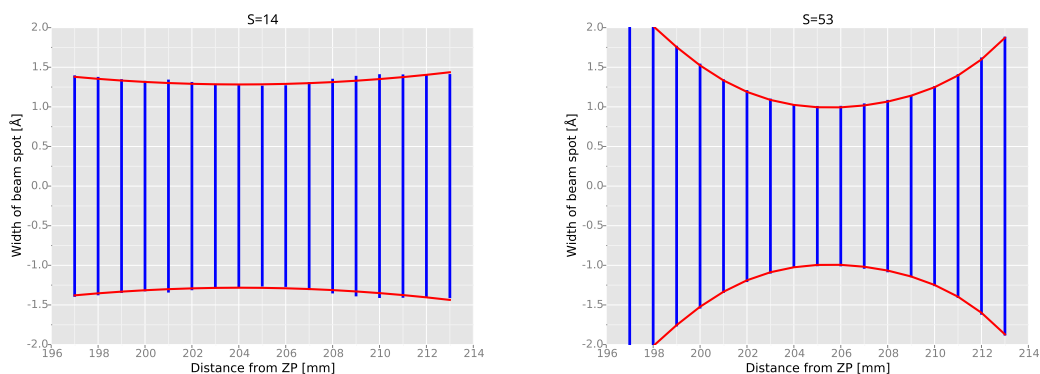

FIGURE 5.2: Plot of chromatic aberration and spot size, with speed ration shown in the plot. The wavelength used is $\lambda = 0.579\,\text{Å}$, which should focus the beam in a distance 205 mm from the zone plate. The blue bars are the FWHM of the spot and the red lines is a polynomial fit to guide the eye. The radius of the source and skimmer were equal for this plot is $r_{\text{Nozzle}} = r_{\text{Skimmer}} = 5\,\mu m$.

Another important thing to visualise is that the beam focus is extremely dependent on the wavelength. If e.g. the wavelength decreased by 0.01 Å, the focus

---

[12]$\Delta\theta = \theta_{\text{in}} - \theta_{\text{out}}$ but since θ_{out} is negative this is equal to the total change in the rays angle $\Delta\theta = \theta_{\text{in}} + |\theta_{\text{out}}|$.

[13]See section 4 and appendix B.1.

spot is moved almost 5 mm to a distance 210 mm from the zone plate. This is illustrated in FIGURE 5.3. This effect is not as significant for lower speed ratios as it is for higher speed ratios, as the change in spot size is not as fast over distances of millimetres.
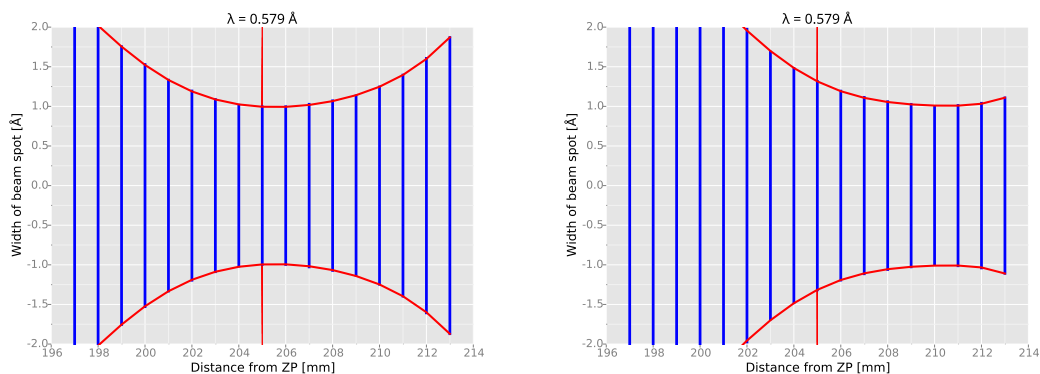

FIGURE 5.3: Plot of chromatic aberration and spot size similar to FIGURE 5.2. This plot illustrates the significant change in focus distance when the wavelength is changed only a little bit. The red line indicates 205 mm from the zone plate i.e the sample plane in the real instrument. The constants for both plots are: $r_{\text{Nozzle}} = r_{\text{Skimmer}} = 5\,\mu\text{m}$ and $S = 53$

5.2 COMPARISON BETWEEN THE SIMULATION AND REAL DATA.

In FIGURE 5.4 data taken with NEMI, demonstrating focusing with a Fresnel zone plate, is compared with the simulation performed here. The results have been normalised for comparison. The simulated data is just a measurement of the intensity of the beam at the focus 203 mm from the zone plate. The geometry of the simulation is the one shown in FIGURE 4.1. Whereas the experimental data is obtained by scanning a 10 µm slit across the focus. This is one of the reasons why the experimental data appears broader than the simulated. The slit could of course be implemented in the simulation, although it was not due to limited time.

What the simulation does provide is an explanation for the puzzling effects in the data. The peaks in the experimental data are all quite similar in width, with no visible narrowing as the speed ratio increases. The simulations show that the reason for this is that the actual focus for all speed ratios is well below the 10 micron width of the slit. Further, the simulations show that the slight change in wavelength with increasing pressure, which increases the speed ratio[5, 12], is enough to cause a broadening of the peak. This was not predicted by the geometrical model[12].
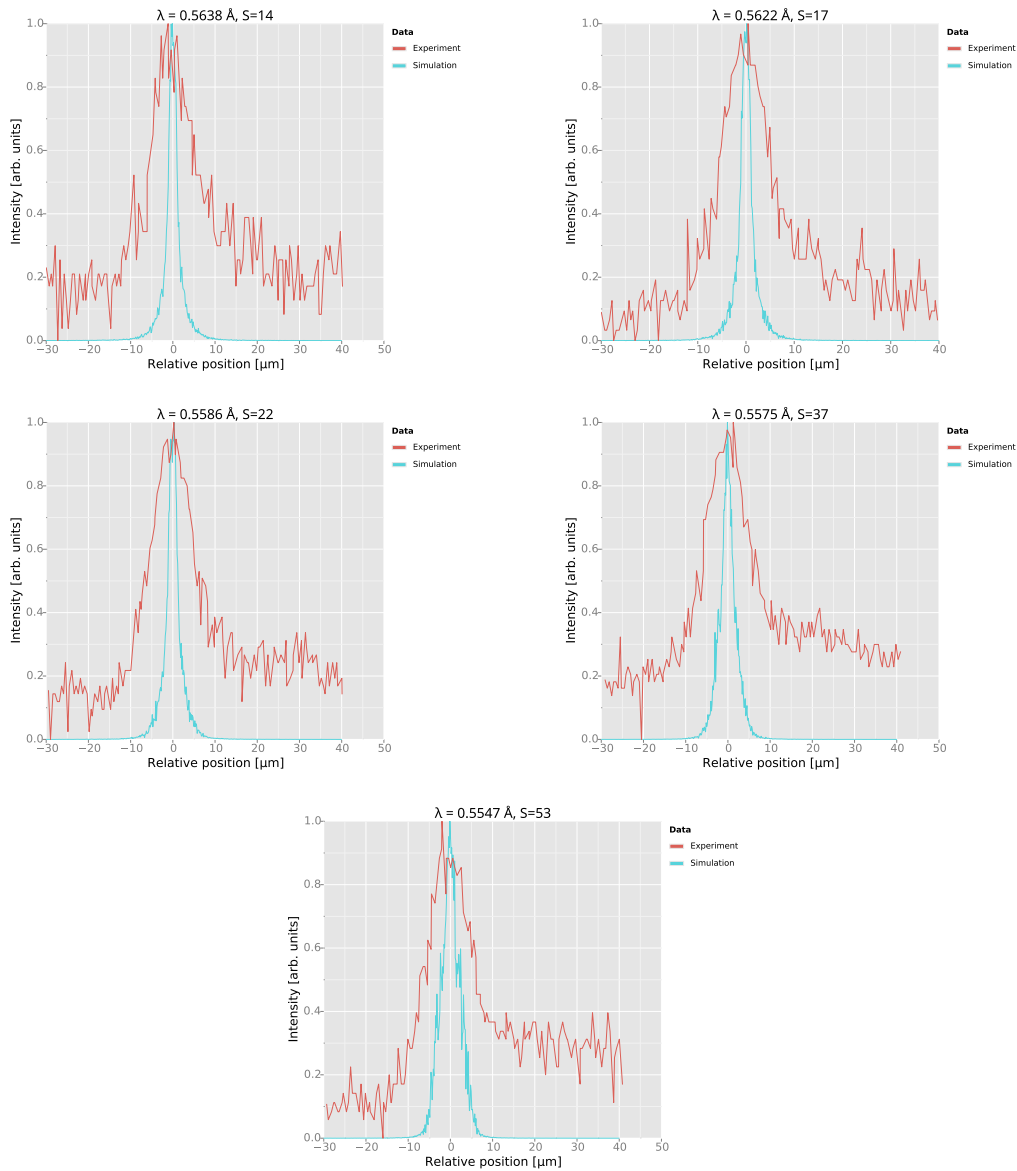
FIGURE 5.4: Plots of the data taken on NEMI superimposed on a simulation with the same parameters as the experiment. The speed distribution and median wavelength for the different plot is shown. The experimental data was obtained by scanning a 10 μm slit across the beam focus, while the simulated data is just the beam intensity at 205 mm from the zone plate.

5.3 A NOTE ON THE ZONE PLATE COMPONENT

It should be noted that the zone plate component written for this simulation is a rough approximation of what actually happens at a zone plate. Instead of just sending all rays to the fist-order focus, there could have been implemented Monte Carlo choices with rays also going to the other orders of focus to more accurately depict the physics of a zone plate. But since I, for this project, am only interested in what happens at the focus, with the focused helium atoms, I decided to make the, to me, simplest possible deterministic approximation to accommodate this. The result was the thin lens approximation.

6. CONCLUSION

The aim of this work was to modify the neutron ray-tracing tool McStas for helium physics, and use it to simulate the neutral helium atom microscope NEMI. This has been done, and the results of the sanity test show that the desired physics is implemented correctly. It also visualises the important property of the focal length: Small changes in the wavelength of the oncoming rays alter the focal length drastically. For example the change of $0.01\,\text{Å}$ in wavelength, from $0.579\,\text{Å}$ to $0.569\,\text{Å}$, results in a change in the focal length of about $5\,\text{mm}$. And this is important, because it provides us with an explanation of why there is no visible peak narrowing in the experimental data as the speed ratio increases. As the speed ratio increases the the wavelength decreases, resulting in peak broadening rather than narrowing. This is shown in the simulations of the experiment.

All in all using a Monte Carlo tool such as McStas to simulate helium ray physics is indeed viable, even with the sort of crude approximations used in this project, such as the mass of helium and the properties of the zone plate component. The tiny accomplishments of this project goes to show that the field of helium atom scattering would benefit greatly with such powerful tool as McStas at their disposal.

As for the immediate future, two further steps are planned for this project:

1. The inclusion of a slit in the simulation of the focus, for a more complete comparison with (improved) experimental results. This will be included in a publication that being prepared together with the NEMI team.

2. The extension of the simulation to a complete NEMI microscope with one or more detectors and typical scattering surfaces. This can be an important contribution to understand the first microscopy images which will hopefully be produced in the near future.

References

[1] David Attwood. *Soft X-Rays and Extreme Ultraviolet Radiation: Principles and Applicatoins.* 1st ed. Cambridge University Press, 1999.

[2] S.R. Buss. *3D Computer Graphics: A Mathematical Introduction with OpenGL.* Cambridge University Press, 2003. ISBN: 9780521821032. URL: https://books.google.dk/books?id=LBm1khtUX0cC.

[3] O. Carnal et al. "Imaging and Focusing of Atoms by a Fresnal Zone Plate". In: *Physical Review Letters* 67.23 (Dec. 1991), pp. 3231–3234.

[4] R. B. Doak et al. "Towards Realization of an Atomic deBroglie Microscope: Helium Atom Focusing Using Fresnel Zone Plate". In: *Physical Review Letters* 83.21 (Nov. 1999), pp. 4229–4232.

[5] Sabrina Daniela Eder. "A Neutral Matter Wave Microscope (NEMI): Design and Setup". PhD thesis. University of Bergen, Dec. 2011.

[6] FEI. *Introduction to Electron Mircoscopy.* Booklet. July 2010. URL: www.nanolab.ucla.edu/pdf/Introduction_to_EM_booklet_July_10.pdf.

[7] A.S. Glassner. *An Introduction to Ray Tracing.* Academic Press, 1989. ISBN: 9780122861604. URL: https://books.google.dk/books?id=YPblYyLqBM4C.

[8] J. M. Hammersley and D. C. Handscomb. *Monte Carlo Methods.* Ed. by M. S. Barlett. 2nd ed. Methuen's monographs on applied probability and statistics. London: Methuen & co Ltd., 1975.

[9] Eugene Hecht. *Optics.* Ed. by Adam Black. 4th ed. Pearson: Addison-Weasley, 2002.

[10] Rebecca Howland and Lisa Benatar. *A Practical Guide to Scanning Probe Microscopy.* Ed. by Jezz Leckenby. 1st ed. ThermoMicroscopes, Mar. 2000.

[11] D.C. Joy. *Helium Ion Microscopy: Principles and Applications.* Briefs in Materials. Springer New York, 2013. ISBN: 9781461486602. URL: https://books.google.dk/books?id=bVm-BAAAQBAJ.

[12] M. Koch et al. "Imaging with neutal atoms - a new matter-wave microscope". In: *Journal of Microscopy* 299.1 (2007), pp. 1–5.

[13] Kim Lefmann et al. "On Monte Carlo ray-tracing simulation of neutron scattrng samples". Apr. 2011.

[14] A. Lipson, S.G. Lipson, and H. Lipson. *Optical Physics.* Cambridge University Press, 2010. ISBN: 9781139492607. URL: https://books.google.dk/books?id=aow3o0dhyjYC.

[15]   Nobleprize.org. *The Nobel Price in Chemestry*. Online. May 2015. URL: http://www.nobelprize.org/nobel_prizes/chemistry/laureates/2014/ (visited on 05/25/2015).

[16]   H. Pauly. *Atom, Molecule, and Cluster Beams I: Basic Theory, Production and Detection of Thermal Energy Beams*. Atom, Molecule, and Cluster Beams. Springer, 2000. ISBN: 9783540669456. URL: https://books.google.dk/books?id=Lwh1uDMAwDgC.

[17]   A. Van Helden, S. Dupré, and R. van Gent. *The Origins of the Telescope*. Geschiedenis Van De Wetenschap in Nederland. KNAW Press, 2010. ISBN: 9789069846156. URL: https://books.google.dk/books?id=XguxYlYd-9EC.

[18]   Peter K. Willendrup et al. *Component Manual for the Neutron Ray-Tracing Package McStas, version 2.1*. DTU. 2800 Kongens Lyngby, Denmark, Sept. 2014.

[19]   Peter K. Willendrup et al. *User and Programmers Guide to the Neutron Ray-Tracing Package McStas, Version 2.1*. DTU. 2800 Kongens Lyngby, Denmark, Sept. 2014.

A. Detailed description of the code

A.1 The Fresnel zone plate (FZP)

The FZP takes four input:

- `rad`: R, t he radius of the FZP (m).

- `dr`: Δr, the width of the outermost transmission zone (m).

- `bs0rad`: The radius of the 0-order beam-stop (default=0 m) (m).

- `cut`: The probability of transmission cut-off (default=0) (1).

<u>First</u> it checks if the rays are too improbable to be transmitted by absorbing the rays with a p-value less than `cut`. <u>Next</u> it checks if the rays hit the centre beam-stop or outside of the FZP and absorbs those.

Now only the transmitted rays are scattered. To figure out how they are scattered, the FZP is approximated by a thin lens to sidestep the fact that the FZP is in fact a wave-optical element that works by diffraction of waves in contrast to a lens that works by refracting rays.

In matrix formulation (detailed in [9]) the thin lens is represented as

$$\begin{bmatrix} 1 & 0 \\ -1/f & 1 \end{bmatrix},$$

where f is the focal length of the lens. When using it on an incoming ray, intercepting the lens at a point x and an angle θ from perpendicular to the lens plane, the resulting ray has the properties

$$\begin{bmatrix} 1 & 0 \\ -1/f & 1 \end{bmatrix} \begin{bmatrix} x \\ \theta \end{bmatrix} = \begin{bmatrix} x \\ \theta - x/f \end{bmatrix}.$$

From this we see that the only property of the ray that changes when it interact with the zone plate is its angle.

To make the calculations easier, the problem is split up in an x- and a y-component. For the x-component we find the angle of incidence θ_x^{in} to be arc tangent between the velocity x-component and z-component

$$\theta_x^{\text{in}} = \text{atan2}\left(v_x, v_z\right).$$

Now, to calculate the change in the angle, we first need get the focal length. Here the focal length of a FZP, assuming no spherical aberration, is used[1]

$$f = \frac{2R\Delta r}{\lambda},$$

where λ is calculated from the ray velocities.

$$\lambda = \frac{2\pi}{4\text{V2K}v}.$$

The V2K is the inbuilt McStas velocity-to-k conversion constant[19] and v is $\sqrt{v_x^2 + v_y^2 + v_z^2}$.

With all these calculations done, the new angle can be calculated. The process for the y-component is the same and the new velocities are calculated as

$$v_x^{\text{out}} = v_x^{\text{in}} \sin \theta_x^{\text{out}}$$
$$v_y^{\text{out}} = v_y^{\text{in}} \sin \theta_y^{\text{out}}$$
$$v_z^{\text{out}} = v_z^{\text{in}} \cos \theta_z^{\text{out}}$$

Since the x- and y-component generally gives different values for θ^{out} the circular mean of the two is used as θ_z^{out} in the final value and outputted to the simulation.

$$\theta_z^{\text{out}} = \text{atan2} \left(\frac{\sin \theta_x^{\text{out}} + \sin \theta_y^{\text{out}}}{2}, \frac{\cos \theta_x^{\text{out}} + \cos \theta_y^{\text{out}}}{2} \right).$$

A.2 THE SOURCE

The source is a parametrised continuous source for modelling a (square or circular) source with (up to) 1 Lorentzian distribution in wavelength and 1 Gaussian distribution in space. The source produces a continuous spectrum. The sampling of the He-atoms is uniform in wavelength.

The source component has 16 input parameters, however a maximum of 11 are used at one time. The 16 inputs are:

- `size` Used if the source output is square (m).

- `yheight` The height of a rectangular source (m).

- `xwidth` The width of a rectangular source (m).

- `rad` The radius of a circular source (m).

- `dist` The distance to the focus of the simulated rays (m).

- `focus_rad` The radius of a circular focus for the simulated rays (m).

- `focus_xw` The width of a square focus for the simulated rays (m).

- `focus_yh` The height of a square focus for the simulated rays (m).

22

- `I1` Flux as the number of atoms per wavelength per square millimetre per steradians. $(\text{Å}^{-1}\,\text{mm}^{-2}\,\text{sr}^{-1})$.

- `target_index` If there is not set a `dist` parameter, the calculate the distance and focus size of the target component with index n

- `lambda_m` λ_0 The mean of the wavelength distribution (Å).

- `S` Speed ratio of the velocity distribution.

- `dlambda` $\Delta\lambda$ The FWHM of the wavelength distribution (Å).

- `Lmin` $\lambda_{\min}$ The lower boundary of the wavelength distribution (Å).

- `Lmax` $\lambda_{\max}$ The upper boundary of the wavelength distribution (Å).

- `Gsigma` The σ of the spatial distribution (m). (If zero, uniform distribution is assumed.)

<u>First</u> it checks whether or not all parameters are set. If $\Delta\lambda$ is not set and S is set then $\Delta\lambda$ is calculated from the formula[5]:

$$\Delta\lambda = 2\sqrt{\ln 2}\,\lambda_0 S^{-1} \tag{13}$$

<u>Next</u> if $\lambda_{\min}$ and $\lambda_{\max}$ is not set then $\lambda_{\min}$ is set to $\lambda_0 - \Delta\lambda$ and $\lambda_{\max}$ is set to $\lambda_0 + \Delta\lambda$. Finally the parameter γ is defined $\gamma = \Delta\lambda/2$.

For every ray an origin is randomly chosen from a uniform distribution on the chosen geometry and the weight factor (which measures the probability of the ray making it to the end) and corrected with the Gaussian spatial distribution centred around $x = 0$ (if set).

$$\mathcal{G}(x;\sigma) = \frac{1}{\sigma\sqrt{2\pi}}e^{\frac{-x^2}{2\sigma^2}} \tag{14}$$

Then the direction of the ray is randomly chosen on the geometry of the focus. Then the wavelength is chosen uniformly on the range $\lambda_{\min}$ to $\lambda_{\max}$ and the velocity of the rays are set.

Finally the weight is corrected with terms for target focusing, wavelength range and Lorentzian distribution (15) and the source area.

$$\mathcal{L}(\lambda;\lambda_0,\gamma) = \frac{1}{\pi\gamma}\frac{\gamma^2}{(\lambda - \lambda_0)^2 + \gamma^2} \tag{15}$$

23

B. The Code

B.1 NEMI.INSTR

```
1  DEFINE INSTRUMENT nemi()

   TRACE

   COMPONENT source = Source_Lorentz_He(
6    rad = 0.000005,
     lambda_m = 0.5793407771852486790086772426077624891119173215,
     S=53,
     Lmin=0.01,
     Lmax=1.08,
11   I1 = 1000000,
     focus_rad = 96e-6,
     dist = 0.935,
     Gsigma = 5e-6)
     AT (0,0,0) ABSOLUTE
16
   COMPONENT skimmer = Aperture(radius=5e-6) AT (0,0,0.01) ABSOLUTE

   COMPONENT slit_1 = Aperture(radius=0.0025,cut=0) AT (0,0,0.717) RELATIVE skimmer

21 COMPONENT zp1 = FZP_simple(bs0rad = 25e-6,
     dr = 51e-9, rad = 96e-6) AT (0,0,0.935) RELATIVE skimmer
   EXTEND
   %{
     if (!SCATTERED) ABSORB;
26 %}

   COMPONENT slit_2 = Aperture(radius=0.0025,cut=0) AT (0,0,1.011) RELATIVE skimmer

   COMPONENT bs_2 = Aperture(radius=20e-6) AT (0,0,1.097) RELATIVE skimmer
31
   COMPONENT sng1 = PSD_monitor_He(filename="d_zp_205mm_S53_dr51_sd10000n.psd",
     xmin=-0.000030,xmax=0.000040,yheight=0.0000010,nx = 500,ny = 1)
     AT (0, 0, 1.140) RELATIVE skimmer

36 END
```

B.2 Source_Lorentz_He.comp

```
DEFINE COMPONENT Source_Lorentz_He
DEFINITION PARAMETERS ()
SETTING PARAMETERS (
  size=0,
  yheight=0,
  xwidth=0,
  rad=0,
  Lmin=0,
  Lmax=0,
  dist,
  focus_rad = 0,
  focus_xw = 0,
  focus_yh = 0,
  I1,
  int target_index=+1,
  lambda_m=0,
  dlambda=0,
  Gsigma,
  S)

OUTPUT PARAMETERS (L,G,l_range,w_mult,w_source,h_source)

/* Helium parameters: (x,y,z,vx,vy,vz,t,sx,sy,sz,p) */

DECLARE
%{
  double l_range, w_mult;
  double w_source, h_source;

  double G(double a, double delta) // A normalized Gaussian dist centerd at 0
  {
    double normfactor = 1/(delta*sqrt(2*PI));
    return normfactor*exp(-(a*a)/(2*delta*delta));
  }

  double L(double l, double l0, double dl) // A normalized Lorentian distribution : ←
      integral over all l = 1
    {
      double gamma2 = dl*dl;
      double normfactor = 1.0/(PI*dl);
      return normfactor*gamma2/((l-l0)*(l-l0)+gamma2);
    }
%}

INITIALIZE
%{
  if (target_index && !dist)
  {
    Coords ToTarget;
    double tx,ty,tz;
    ToTarget = coords_sub(POS_A_COMP_INDEX(INDEX_CURRENT_COMP+target_index),←
        POS_A_CURRENT_COMP);
    ToTarget = rot_apply(ROT_A_CURRENT_COMP, ToTarget);
    coords_get(ToTarget, &tx, &ty, &tz);
    dist=sqrt(tx*tx+ty*ty+tz*tz);
  }
  if (rad > 0) {
```

```
   w_mult = 2*PI*rad*rad*1.0e4;      /* source area correction */
} else if (size>0) {
   w_source = h_source = size;
   w_mult = w_source*h_source*1.0e4;      /* source area correction */
} else {
   w_source = xwidth;
   h_source = yheight;
   w_mult = w_source*h_source*1.0e4;      /* source area correction */
}
if (dlambda == 0 && S){
   dlambda = 2*sqrt(log(2))*lambda_m/S;
}
if (Lmax == 0 && Lmin == 0) {
   Lmin=lambda_m-dlambda;
   Lmax=lambda_m+dlambda;
}
l_range = Lmax-Lmin;
w_mult *= l_range;                /* wavelength range correction */
w_mult *= 1.0/mcget_ncount();   /* correct for # neutron rays */

if (w_source <0 || h_source < 0 || Lmin <= 0 || Lmax <= 0 || dist <= 0 || I1 <= 0 )↩
      // || T2 <= 0|| T3 <= 0)
{
   printf("Source_Lorentz_test: %s: Error in input parameter values!\n"
          "ERROR           Exiting\n", NAME_CURRENT_COMP);
   exit(0);
}

%}

TRACE
%{
   double v,tau_l,E,lambda,k,r,xf,yf,dx,dy,dOmega,rho;
   double angle;

   p=1;
   t=0;
   z=0;
   if (rad > 0) {
      angle = 2*PI*rand01();
      rho = rad*sqrt(rand01());
      x = rho*cos(angle);
      y = rho*sin(angle); // Choose Initial posotion
   } else {
      x = 0.5*w_source*randpm1();
      y = 0.5*h_source*randpm1();           /* Choose initial position */
      rho = sqrt(x*x+y*y);
   }
   if (Gsigma > 0) {
      p *= G(rho,Gsigma);// corrected for nozzel gaussian output.
   }
   if (focus_rad > 0) {
      randvec_target_circle(&xf, &yf, &r, &dOmega,0, 0, dist,focus_rad);
   } else {
      randvec_target_rect_real(&xf, &yf, &r, &dOmega,
               0, 0, dist, focus_xw, focus_yh, ROT_A_CURRENT_COMP, x, y, z, 2);
   }
   dx = xf-x;
   dy = yf-y;
   r = sqrt(dx*dx+dy*dy+dist*dist);
```

```
      lambda = Lmin+l_range*rand01();     /* Choose from uniform distribution */
      k = 2*PI/lambda;
      v = K2V*k/4;   // compensation for the mass of helium.
119
      vz = v*dist/r;
      vy = v*dy/r;
      vx = v*dx/r;

124   p *= w_mult*dOmega;                  /* Correct for target focusing etc */

      double gamma = dlambda/2;
      p *= I1*L(lambda,lambda_m,gamma);   // corrected for speed distribution.

129 %}

    MCDISPLAY
    %{
      magnify("xy");
134   multiline(5, -(double)focus_xw/2.0, -(double)focus_yh/2.0, 0.0,
                    (double)focus_xw/2.0, -(double)focus_yh/2.0, 0.0,
                    (double)focus_xw/2.0,  (double)focus_yh/2.0, 0.0,
                   -(double)focus_xw/2.0,  (double)focus_yh/2.0, 0.0,
                   -(double)focus_xw/2.0, -(double)focus_yh/2.0, 0.0);
139   if (dist) {
        dashed_line(0,0,0, -focus_xw/2,-focus_yh/2,dist, 4);
        dashed_line(0,0,0,  focus_xw/2,-focus_yh/2,dist, 4);
        dashed_line(0,0,0,  focus_xw/2, focus_yh/2,dist, 4);
        dashed_line(0,0,0, -focus_xw/2, focus_yh/2,dist, 4);
144   }
    %}
    END
```

B.3 FZP_simple.comp

```
DEFINE COMPONENT FZP_simple
DEFINITION PARAMETERS ()
SETTING PARAMETERS (
  rad ,
  dr ,
  bs0rad = 0,
  cut = 0)
OUTPUT PARAMETERS ()

/* Helium parameters: (x,y,z,vx,vy,vz,t,sx,sy,sz,p) */

TRACE
%{

  double focal_point,rho,lambda,vel,theta_inx,theta_iny,theta_outx,theta_outy;

  PROP_Z0;
  if ((bs0rad != 0) && (x*x + y*y < bs0rad*bs0rad))
    {ABSORB;}
  else if (p < cut)
    {ABSORB;}
  else if (x*x + y*y < rad*rad)
    {SCATTER;
      vel=sqrt(vx*vx+vy*vy+vz*vz);
      lambda = 2*PI/(4*V2K*1e10*vel); // A factor of 10^10 to go from Å to m
      focal_point = 2*rad*dr/lambda; //-dr*dr/lambda; //add this to calculate w/ ↵
          spherical aberration

      theta_inx = atan2(vx,vz);
      theta_iny = atan2(vy,vz);
      theta_outx = theta_inx - x/focal_point;
      theta_outy = theta_iny - y/focal_point;
      vx = vel*sin(theta_outx);
      vy = vel*sin(theta_outy);
      theta_outz = atan2(0.5*(sin(theta_outx)+sin(theta_outy)),0.5*(cos(theta_outx)+↵
          cos(theta_outy)));
      vz = vel*cos(theta_outz);
      p *= 0.10;
    }
%}

END
```